energies

MDPI

Article

Study on the Influence and Control of Stress Direction Deflection and Partial-Stress Boosting of Main Roadways Surrounding Rock and under the Influence of Multi-Seam Mining

Dongdong Chen, Fangfang Guo, Zijian Li, Xiang Ma, Shengrong Xie *, Yiyi Wu and Zhiqiang Wang

School of Energy and Mining Engineering, China University of Mining & Technology-Beijing, Beijing 100083, China
* Correspondence: xsrxcq@cumtb.edu.cn

Abstract: A large coal pillar (usually more than 90 m) is generally left in place to ensure the stability of main roadway groups, due to its long service lifespan, which commonly also causes a significant loss of coal resources. The design of the width of the protective coal pillar and the control system of the surrounding rock are directly determined by the characteristics of the stress field and the damage mechanism under the influence of the mining activities. However, there are few studies on the effects of the partial-stress boosting and the direction deflection of the stress field on the failure evolution of the surrounding rock (especially in multi-seam mining). In this paper, theoretical analysis and numerical simulation are used to investigate the direction evolution of the maximum principal stress in front of the working face with malposition distances between the upper and lower working faces during the influence of double coal seams mining. Furthermore, a large-scale numerical model is used to study the deviatoric stress evolution of the surrounding rock and the propagation process of the plastic zone in the main roadway group with different widths of protective coal pillars. Then, an asymmetric cooperative anchoring classification method is proposed to strengthen the roadway support, depending on the critical area of the deviatoric stress in the roadway surrounding rock. The peak zone deflection of the deviatoric stress determines the evolution direction of the plastic area, and the peak value of the deviatoric stress presents a typical asymmetric stress boosting on both sides of the roadway. These findings are validated by the on-site ground pressure monitoring results and the practical failure modes of the surrounding rock.

Keywords: main roadway group; mining-induced stress; surrounding rock stability; ground control; deflection of principal stress

Citation: Chen, D.; Guo, F.; Li, Z.; Ma, X.; Xie, S.; Wu, Y.; Wang, Z. Study on the Influence and Control of Stress Direction Deflection and Partial-Stress Boosting of Main Roadways Surrounding Rock and under the Influence of Multi-Seam Mining. *Energies* **2022**, *15*, 8257. https://doi.org/10.3390/en15218257

Academic Editor: Nikolaos Koukouzas

Received: 10 October 2022
Accepted: 2 November 2022
Published: 4 November 2022

1. Introduction

Energy and mineral resources serve as the economic development drivers for countries around the world [1]. China's proven coal resource reserves rank second in the world, and the total consumption of coal in China's primary energy consumption in 2020 still accounts for more than 50% of the proportion [2,3]. Ensuring the safe production of coal means a stable economic development. Long-wall underground mining arose in Europe and is widely used in China because of its high productivity. About 85 percent of China's coal production comes from underground, and long-wall mining is used for most of it, about 20 percent of the total; and about 5 percent of India's production comes from underground [4–7]. Although long-wall mining has a high productivity, because of the characteristics of roadway layout, large coal pillars should be set in terminal stage of long-wall face to ensure the safety of the roadway group [8]. Due to the long service life of the main roadway group, the mine tends to set up excess coal pillars to maintain the main roadway safety, so the study on the width of the roadway protective coal pillar is important.

The main roadways are the lifeblood of mine transportation, ventilation, pedestrians, etc., and they generally need to serve the whole production process of the mine. Therefore,

most of the main roadways are built on the roof or floor of the coal seam in underground mining. Furthermore, the coal seam roadways are easy to excavate, and coal resources can be recovered as soon as possible, reducing the financial pressure on mine production. In recent years, the main roadways are increasingly inclined to be placed in coal seams in some mine areas with relatively good geological conditions, such as in Yulin and Erdos, China.

For the roadway problems of a coal mine, scholars around the world have made many efforts to study the properties of the roadway surrounding rock, the state of the deposit, the influence of mining stress, the mechanism of the surrounding rock deformation, and the role of support, etc., and have accumulated rich theoretical and practical engineering experience. Gao et al. [9–11] conducted a series of numerical simulations to study the roadway's squeezing failure and shear failure, using the UDEC Trigon method and analyzed the effects of rock bolts on the roadway support. Wang et al. [12] tested the properties of surrounding rock considering the influence of the lower coal seam on the stress state by a numerical simulation. The creep characteristics of the surrounding rock of the mining roadway and its effects on the deformation were systematically performed. Pan et al. [13] focused on the deformation and failure process and the mechanism of the surrounding rock induced by the stress adjustment in a deeply arched roadway. A self-developed large-scale simulation test was carried out. Mohammadi et al. [14] developed a geometric computational model to calculate the extension of the excavation-damaged zone above the gate roadways, induced by longwall mining and proposed a new mathematical formulation to determine the face influence coefficient.

Huang et al. [15] clarified the connotation of roadway mining and large deformation under the consideration of the deviatoric stress. They proposed a theoretical framework of a large deformation of surrounding rock rheology and structural instability in deep mining roadways. Y et al. [16] investigated the problems of roadway stability with repeated mining-induced disturbance and focused on the direction and emphasis of the stability control of roadway surrounding rock. Shan et al. [17] summarized the current research status of coal tunnel support technology at home and abroad, in recent years.

Moreover, they proposed that roadway support adopted a more diversified integrated active support technology and showed the trend of gradually moving into intelligent support. Some researchers [18–24] concentrated on the significant deformation of the surrounding rock in deep roadways and targeted control technologies were proposed to solve this problem. These papers are dedicated to discovering the failure mechanism of the roadway or efficient roadway support technology to prevent the instability of the roadway. The Coal pillar width does contribute an essential part to the stability of the roadway. The non-pillar technologies (gob-side entry driving or gob-side entry retaining) have been widely used in China, due to the high coal resource recovery rate [25–32]. Currently, for a coal seam main roadway group in China, the protective coal pillar is usually larger than 90 m for the stability of the roadway, which causes a tremendous waste of coal resources. Some experts have also studied the width of coal pillars to protect the main roadways. For example, some scholars [33,34] studied the stability control of the main deep roadway groups, considering the characteristic rheology coupled with multiple disturbances of mining activities of the adjacent working faces. It determined that it was rational to leave a protective coal pillar for main roadway groups with a width of 100 m.

However, at present, for the close multi-seam mining, when the width of the end-mining coal pillar of each coal seam is different, the stress superposition and direction deflection law in the area in front of the working face, caused by the influence of mining and the evolution law of the damage to the main roadway surrounding rock, is rarely studied. Therefore, it is impossible to determine the location of the high deviatoric stress area and the critical control orientation of the main roadway surrounding rock. This also leads to the roadway surrounding rock support design that is not a targeted basis.

The study background of this paper is to examine the specific engineering geological conditions of close two-seam coal mining and the different widths of end-mining coal pillars. On this basis, the following studies are conducted: the law of the principal stress

direction deflection and plastic damage evolution in the main roadway surrounding rock, the stress superposition and deflection of the peak deviatoric stress area. Through the study, the location of critical high deviatoric stress zones and support orientation of the roadway surrounding rock are obtained, and the asymmetric reinforcement support technology of the channel steel-anchor cable truss with a bi-directional reinforcement function is proposed. The experimental results show that the technique is effective.

2. Project Overview

2.1. Geological Conditions

The No.3 and No.4 coal seams are mainly exploited in the mine, and the No.4 coal seam is located 25 m above the No.3 coal seam. The relationship between the two coal seams is shown in Figure 1. Both are near horizontal coal seams adopting the comprehensive mechanized top coal caving mining method. The thickness of the No.4 coal seam is about 7.5 m, which has been recovered, and a 90 m coal pillar was left to ensure the stability of the main roadway group. The geological histogram of the long-wall working face (LWF) 8216 is shown in Figure 1. The long-wall working face (LWF) 8216 in the No.3 coal seam under the residual coal pillar is the main mining face, with an average coal seam thickness of about 5.5 m and a burial depth of about 400 m. The spacing between the two adjacent roadways is 30 m, and there is slight deformation in the surrounding rock of the roadway group during the upper coal seam recovery. Therefore, during the retreating of the lower coal seam, the mine intended to further reduce the width of the protective coal pillar for the roadway group to maximize the recovery of coal resources. The location of the project is shown in Figure 2.

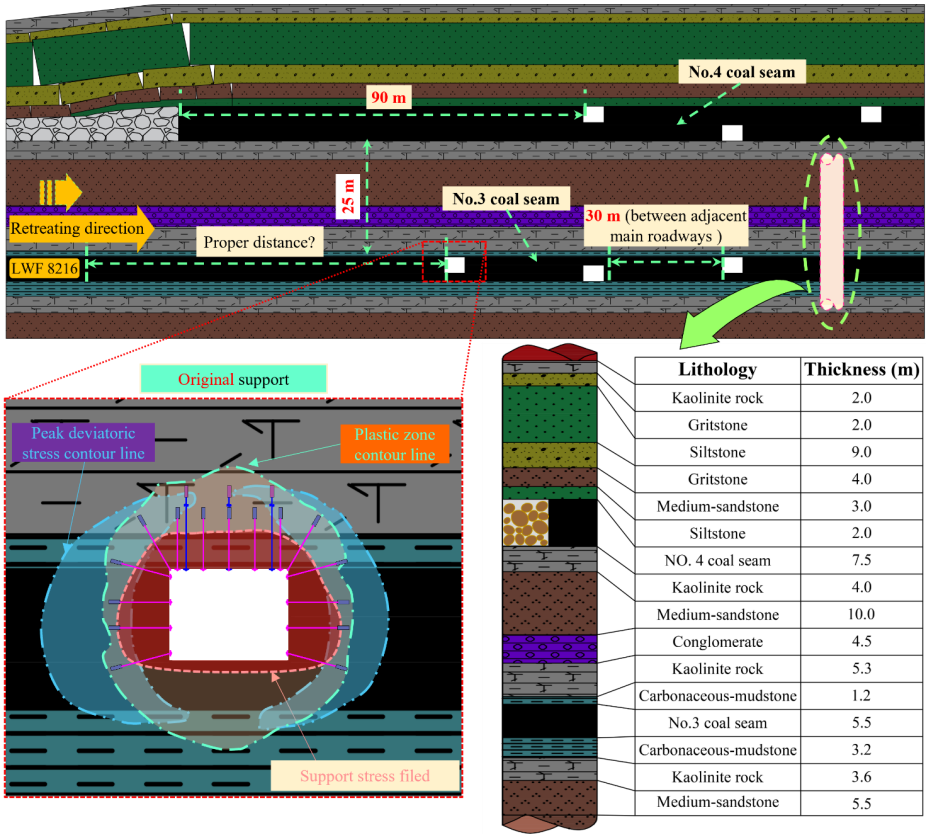

Figure 1. Main roadway group layout of the multiple coal seam and generalized stratigraphic column in the test site.

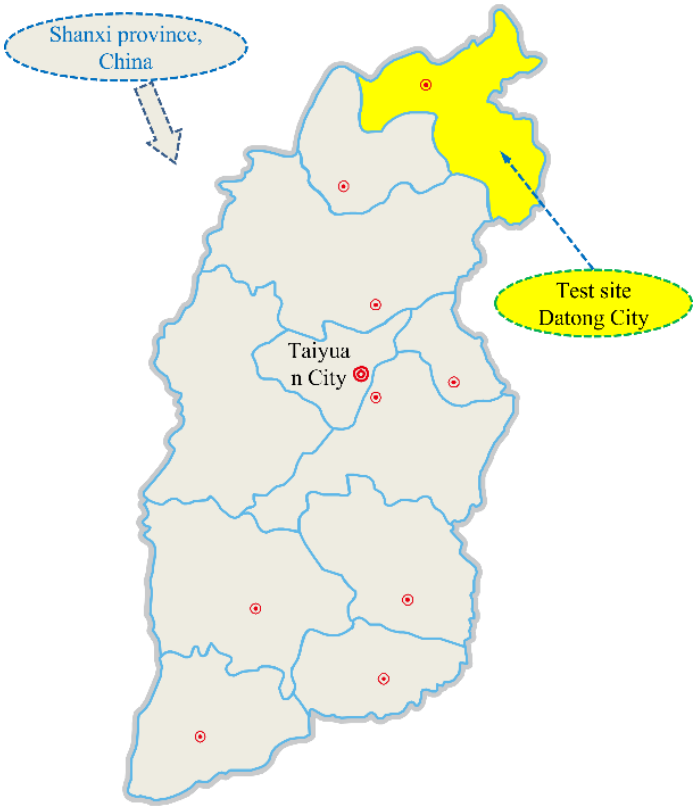

Figure 2. Location of the Project.

2.2. Description of the Mining Conditions

The No.4 coal seam above the longwall working face 8216 of the No.3 coal seam in the mine has been mined out, and the width of the protective coal pillar of the main roadway group is 90 m. During the mining process of the No.3 coal seam, it usually chooses a giant protective coal pillar (90 m~140 m) to avoid the damaging effect with multi-seam mining stress disturbance to the main roadway. The main roadway is supported by a symmetrical anchor bolting and cable combination using a large coal pillar width. The anchor cables are Φ17.8 × 7000 mm with an inter-row distance of 1500 × 3000 mm and pallet size of 300 × 300 × 16 mm (length × width × height); the anchor bolts are left hand non-longitudinal rebar threaded steel anchor bolts with Φ20 × 2400 mm and inter-row distance of 900 × 1000 mm, and the pallet is a dished pallet with 150 × 150 × 10 mm (length × width × height). The roof, floor, and two ribs of the roadway use a shotcrete support. The roof and two ribs' concrete thickness is 100 mm, and the concrete grade is C20. The support parameters of the main return-air roadway and main haulage roadway are shown in Figure 3.

Although the giant protective coal pillar prevented the main roadway group from destruction and instability, it also caused the loss of coal resources. In addition, the asymmetrical damage to the main roadway can occur under symmetrical anchor rope support conditions after the suspension of mining at specific working faces of the No.3 coal seam. In the ribs of the main return-air roadway and the main haulage roadway, the support structure showed apparent damage, as shown in Figure 4. This is inconsistent with our traditional understanding of the location of the roadway damage. The roadway failure location under the influence of mining stress should first appear in the area near the working face. Therefore, in the study of multi-seam mining conditions, the direction of the evolution of the roadway damage is conducive to the better design of targeted support programs to improve support efficiency.

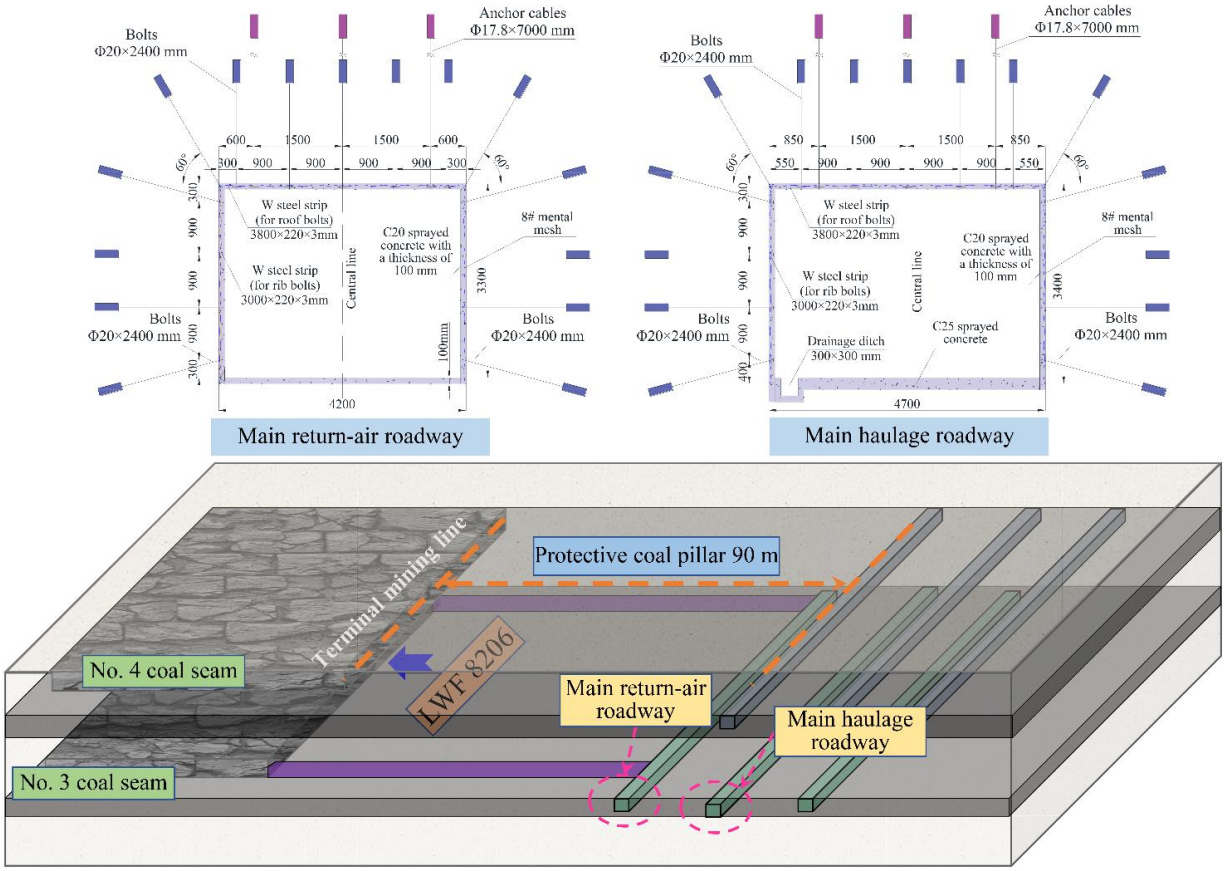

Figure 3. Support parameters of the main roadway group.

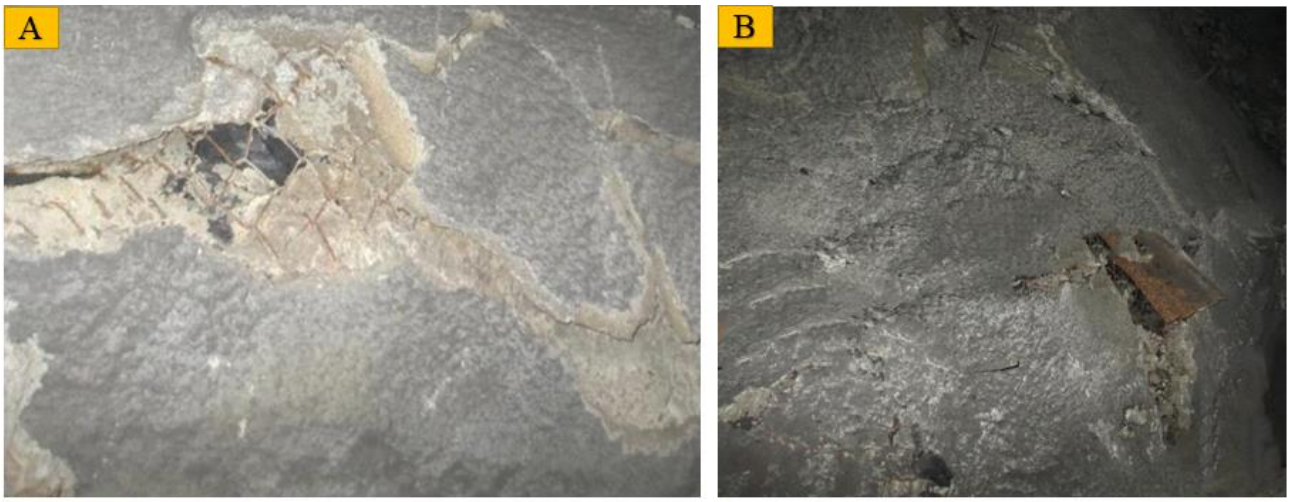

Figure 4. Asymmetric damage of the main roadway after stopping mining. (**A**) main return-air roadway, and (**B**) main haulage roadway.

3. Theoretical Analysis of the Direction Deflection of the Stress and Partial-Stress Boosting in the Surrounding Rock

3.1. Solution for the Direction of Stress Deflection and Partial-Stress Boosting in the Mining Superposition Conditions

The problems of stress distribution and plastic damage depth of a coal mass have been of great concern. Especially the superimposed loading law of the stress field with multi-seam mining, which is an essential guideline for engineering practice.

The traditional view mainly focuses on the change of lead vertical pressure (vertical direction). However, vertical stress only represents one of the nine stress components. The direction is all vertical, so the simple vertical stress cannot scientifically and comprehensively characterize the change of stress in the over-front area, caused by the mining of the working face, and it cannot effectively propose the damage characteristics of the advanced abutment pressure on the main roadway and the critical direction of control.

Deviatoric stress synthesizes three principal stresses, making the analysis more comprehensive and scientific than the single vertical stress index. According to the elastic-plasticity theory [35], the deviatoric stress plays a dominant role in the plastic deformation of the surrounding rock, so the analysis of the mining superposition main roadway surrounding stress increase law by the deviatoric stress index, can more comprehensively reflect the essence of the surrounding rock deformation damage development.

The S_1 is the principal deviatoric stress, which plays a dominant role in the stress tensor, and the commonly referred deviatoric stress refers to the maximum principle of the deviatoric stress, which is also the analytical index of the deviatoric stress in this section, and its formula is as follows.

$$S_1 = \sigma_1 - \frac{\sigma_1 + \sigma_2 + \sigma_3}{3} \tag{1}$$

In the three-dimensional stress field, the magnitude of the principal stress and its direction can be solved by the magnitude of nine (six independent) stress components (σ_{xx}, σ_{yy}, σ_{zz}, τ_{xz}, τ_{xy}, τ_{yz}, τ_{zx}, τ_{zy}, τ_{yx}). Take any unitary body for an oblique section ABC, as in Figure 5, and let the outer normal of the plane ABC be N, whose direction cosine is

$$cos(N,x) = l,\ cos(N,y) = m,\ cos(N,z) = n \tag{2}$$

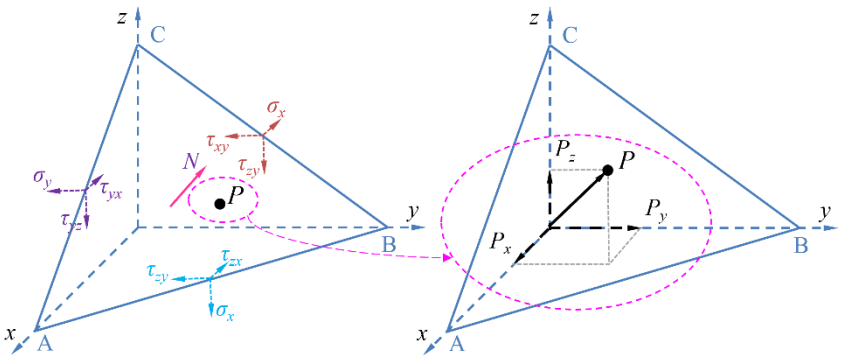

Figure 5. Stress components of the oblique section of the element body.

The full stress P of the triangle ABC can be decomposed into p_x, p_y, p_z, and the following formula is satisfied:

$$\left.\begin{array}{l} p_x = l\sigma_x + m\tau_{yx} + n\tau_{zx} \\ p_y = m\sigma_y + n\tau_{zy} + l\tau_{xy} \\ p_z = n\sigma_z + l\tau_{xz} + m\tau_{yz} \end{array}\right\} \tag{3}$$

Let the positive stress on triangle ABC be σ_N. Then from the projection, we have

$$\sigma_N = lp_x + mp_y + np_z \tag{4}$$

It follows that

$$\sigma_N = l^2\sigma_x + m^2\sigma_y + n^2\sigma_z + 2mn\tau_z + 2nl\tau_{zx} + 2lm\tau_{xy} \tag{5}$$

$$p^2 = \sigma_N^2 + \tau_N^2 = p_x^2 + p_y^2 + p_z^2 \tag{6}$$

Suppose there is a principal stress plane at P, and the projection of the full stress (principal stress σ) on this plane on the coordinate axis is:

$$p_x = l\sigma,\ p_y = m\sigma,\ p_z = n\sigma \tag{7}$$

Satisfies Equation (9)

$$l^2 + m^2 + n^2 = 1 \tag{8}$$

Equation (9) can thus be obtained

$$\left.\begin{array}{l}(\sigma_x - \sigma)l + \tau_{yx}m + \tau_{zx}n = 0\\ \tau_{xy}l + (\sigma_y - \sigma)m + \tau_{zy}n = 0\\ \tau_{xz}l + \tau_{yz}m + (\sigma_z - \sigma)n = 0\end{array}\right\} \tag{9}$$

Following a simplification, Equation (10) can be derived

$$\begin{cases}\tau_{yx}\frac{m_1}{l_1} + \tau_{zx}\frac{n_1}{l_1} + (\sigma_x - \sigma_1) = 0\\ (\sigma_y - \sigma_1)\frac{m_1}{l_1} + \tau_{zy}\frac{n_1}{l_1} + \tau_{xy} = 0\end{cases} \tag{10}$$

The two equations solved for the two unknowns (m_1/l_1) and (n_1/l_1) so that l_1, as well as m_1 and n_1, can be obtained by bringing in the following equation:

$$l_1 = \frac{1}{\sqrt{1 + \left(\frac{m_1}{l_1}\right)^2 + \left(\frac{n_1}{l_1}\right)^2}} \tag{11}$$

l_1, m_1, and n_1 are the cosine of the angle between the principal stress of the principal plane and the three axes. Therefore, based on the nine stress components at any point, the three principal stresses and the direction of the principal stresses can be solved.

3.2. Solution for the Degree of the Stress Direction Deflection and the Partial-Stress Boosting and the Damage Analysis with the Disturbance of Multi-Seam Mining

As shown in Figure 6, the stress components and the changes of the principal stress during the mining of each coal seam can be extracted through a numerical calculation. Then, the changes in the magnitude and direction of the principal stress before and after being affected by the mining superposition at any location, can be obtained. At the same time, as the magnitude of the principal stress and its direction change, the peak area of the deviatoric stress of the roadway surrounding rock is bound to change, which will inevitably lead to asymmetric damage to the surrounding rock. That is, through the size of the principal stress field of the roadway surrounding rock and its direction, changes to determine the critical damage area of the roadway, to guide the determination of the vital reinforcement direction of the roadway.

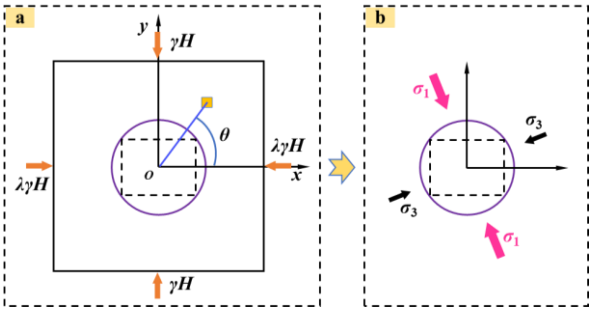

Figure 6. Expression of the principal stresses for the stress components. (**a**) Arbitrary stress field, (**b**) The direction deflection of the principal stress field and the partial-stress boosting.

According to the principal stress field, to solve the damage range of the roadway, using the stress distribution formula around the hole in the elastoplastic mechanics, the stress expression at any point of the surrounding rock of a circular roadway in polar coordinates [36] can be found as follows.

$$\begin{cases} \sigma_r = \left[3(\lambda-1)\cos 2\theta \frac{a^4}{R_\theta^4} + (1+\lambda)\left(1-\frac{a^2}{R_\theta^2}\right) + (\lambda-1)\cos 2\theta - 4(\lambda-1)\cos 2\theta \frac{a^2}{R_\theta^2}\right]\frac{\gamma H}{2} \\ \sigma_\theta = \left[(1+\lambda)\left(1+\frac{a^2}{R_\theta^2}\right) - \cos 2\theta(\lambda-1) - 3\cos 2\theta(\lambda-1)\frac{a^4}{R_\theta^4}\right]\frac{\gamma H}{2} \\ \tau_{r\theta} = \left[\sin 2\theta(\lambda-1) + 2\sin 2\theta(\lambda-1)\frac{a^2}{R_\theta^2} - 3\sin 2\theta(\lambda-1)\frac{a^4}{R_\theta^4}\right]\frac{\gamma H}{2} \end{cases} \tag{12}$$

where: σ_r is the radial stress at any point; σ_θ is the circumferential stress at any point; $\tau_{r\theta}$ is the shear stress at any point; γ is the weight density of rock; H is the burial depth of the roadway; λ is the lateral pressure coefficient; a is the radius of the circular roadway; the polar coordinates of any point are set as (θ, R_θ). In the polar coordinate system, the formula for calculating the principal stress determined by the stress component [36] is:

$$\begin{cases} \sigma_1 = \frac{\sigma_r+\sigma_\theta}{2} + \frac{1}{2}\sqrt{(\sigma_r-\sigma_\theta)^2 + 4\tau_{r\theta}^2} \\ \sigma_3 = \frac{\sigma_r+\sigma_\theta}{2} - \frac{1}{2}\sqrt{(\sigma_r-\sigma_\theta)^2 + 4\tau_{r\theta}^2} \end{cases} \tag{13}$$

The stress state of a point can be decomposed into spherical stress and deviatoric stress, where the deviatoric stress is the dominant factor leading to the plastic deformation of the surrounding rock, so use the deviatoric stress for the theoretical analysis.

When conducting the study of the stress in the roadway enclosure, the problem can be simplified to a plane problem, which results in the principal deviatoric stress calculation formula:

$$S_1 = \frac{\gamma H}{6}(1+\lambda) + \frac{\gamma H a^2(1-\lambda)\cos 2\theta}{3R_\theta^2} + \frac{\gamma H}{2}\sqrt{\left[(1+\lambda)(-\frac{a^2}{R_\theta^2}) + (\lambda-1)(1+3\frac{a^4}{R_\theta^4} - 2\frac{a^2}{R_\theta^2})\cos 2\theta\right]^2 + \left[(\lambda-1)\left(1-3\frac{a^4}{R_\theta^4}+2\frac{a^2}{R_\theta^2}\right)\sin 2\theta\right]^2} \tag{14}$$

The surrounding rock plasticity criterion satisfies the following relation [37,38].

$$\frac{{\sigma_c}^2(\sigma_1+\sigma_3)}{2(\sigma_c+2\sigma_t)} + \frac{\sigma_t{\sigma_c}^2}{\sigma_c+2\sigma_t} - \frac{{\sigma_c}^4}{8(\sigma_c+2\sigma_t)^2} - \frac{(\sigma_1-\sigma_3)^2}{2} = 0 \tag{15}$$

By combining the deviatoric stress formula and its plasticity criterion, we can analyze the location of the high deviatoric stress zone in the roadway surrounding rock. We can also make it possible to quantify the deflection of the high deviatoric stress zone when the principal stress direction changes. Combined with the numerical simulation tests, the evolution of the peak stress zone of the surrounding rock in the roadway, from no stress deflection and partial-stress boosting to stress deflection and partial-stress boosting conditions, is shown in Figure 7.

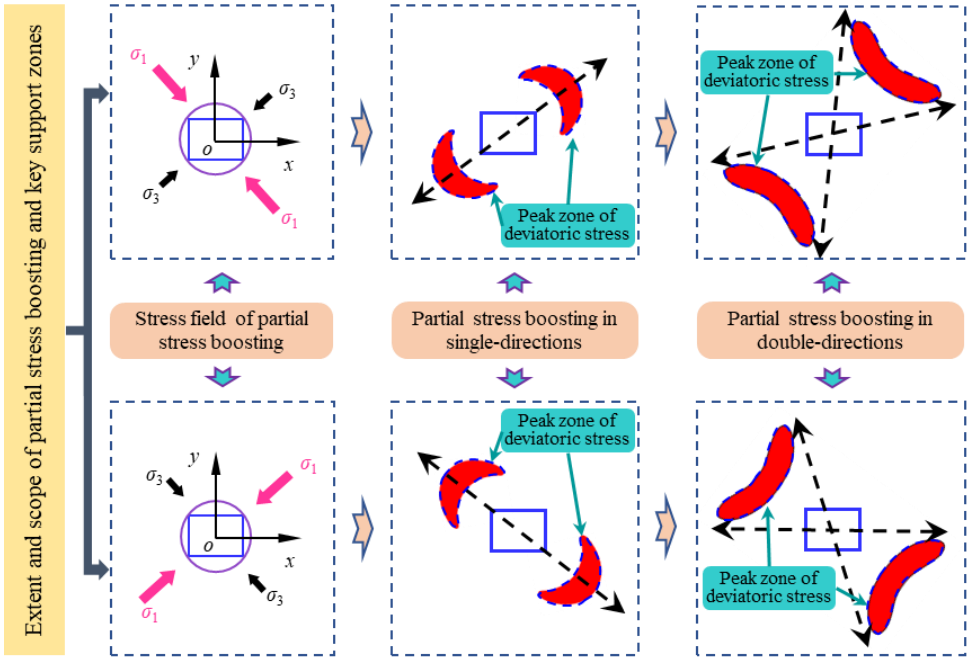

Figure 7. Evolutionary pattern of surrounding rock damage under different stress direction deflection and partial-stress boosting conditions.

With different degrees and directions of stress deflection and partial-stress boosting, there exist different deviatoric stress critical zones in the roadway surrounding rock, and this zone highlights the roadway surrounding rock's key damage development area and direction: When the degree of stress deflection and partial-stress boosting is small, the roadway surrounding the rock's deviatoric stress critical zone mainly develops symmetrically in two directions of the roadway; when the degree continues to increase, the deviatoric stress critical zone is symmetrically distributed on both sides of the roadway surrounding rock, and the damaged area tends to develop from four directions to the deep part of the surrounding rock. Therefore, under stress deflection and partial-stress boosting conditions, the surrounding rock is not gradually and uniformly damaged to the deep part of the surrounding rock, but it is a non-uniform process. The different stress direction deflection and partial-stress boosting conditions lead to two directions of damage development or four directions of the damage development pattern of the surrounding rock, which has an essential guidance significance for the design of the surrounding rock control scheme.

4. Numerical Simulation

The influence with multi-seam mining will cause a stress increase effect on the main roadway. Under different principal stress field conditions, the roadway's stress peak area and damage development area will be deflected, forming the phenomenon of stress deflection and partial-stress boosting. There is an essential difference between the development of the surrounding rock deformation and the critical area of its control. The numerical simulation can more intuitively study the law of the deflected loading of the main roadway surrounding rock, caused by mining multiple coal seams. This is essential for analyzing the plasticization law of the main roadway surrounding rock and determining the critical reinforcement location of the main roadway surrounding rock.

The model selects the LWF 8216 as the test working face. The *X*-axis length is 400 m in the length direction, the *Y*-axis length is 100 m and parallel to the main roadway group, and the *Z*-axis length is 90 m in the vertical direction, as shown in Figure 8. The boundary displacement of the model is constrained in the horizontal and bottom. The upper of the model is subjected to a stress of 7.75 MPa, equivalent to the weight of the overburdened rock, and the lateral stress coefficient is 1.2. The model is calculated using the Mohr–

Coulomb model. In contrast, the double-yield model is used for the job. The mechanical parameters of the coal and rock mass were very important to the accuracy of the numerical simulation results. Cai et al. [39] suggested that the tensile strength, cohesion and elastic modulus of the coal and rock mass could be estimated in the range of 0.10–0.25 times of the experimental results in the laboratory. Mohammad et al. [40] suggested that the average uniaxial compressive strength of the numerical model should be 0.284 of the laboratory strength and the average stiffness should be 0.469 of the laboratory stiffness. Combined with the generalized Hoke–Brown failure criterion [41–43], the simplified physical parameters of the coal seam are shown in Table 1.

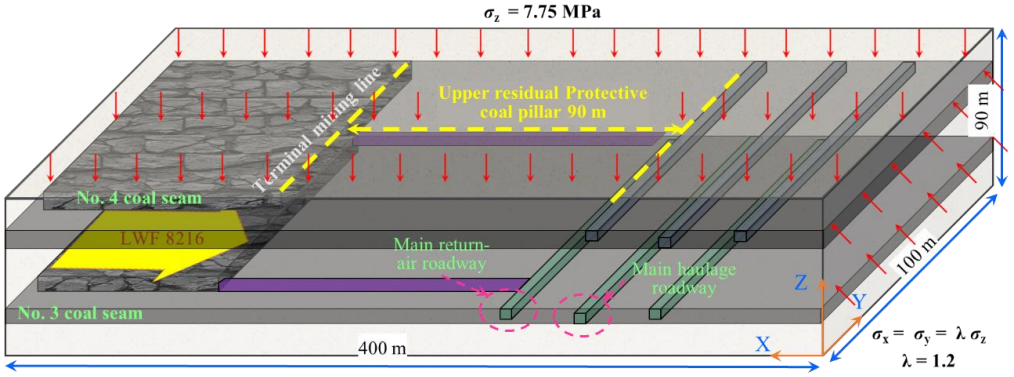

Figure 8. Numerical model overview.

Table 1. Properties of the rock mass in LWF 8216.

Lithology	Density (kg·m^{-3})	Elastic Modulus (GPa)	Friction (°)	Cohesion (MPa)	Tensile Strength (MPa)
Gritstone	2650	17.43	32	3.16	2.42
Siltstone	2602	14.59	35	3.07	2.17
No.4 coal seam	1400	3.79	18	1.49	1.21
Conglomerate	2660	18.08	34	3.5	3.13
No.3 coal seam	1400	3.80	18	1.49	1.21
Carbonaceous-mudstone	2200	14.77	29	2.94	2.22
Kaolinite rock	2570	17.00	38	5.18	2.78
Medium-sandstone	2557	12.69	38	6.26	3.63

The numerical model is used to study two aspects: (1) The change of the abutment pressure in front of the working face when the upper and lower coal seams are in different positions (outer fault, overlap, internal fault). (2) To investigate the stress distribution and the mechanism of the surrounding rock damage in the surrounding rock of the roadway when the width of the coal pillar is different in the working face of the lower coal seam, when the protective pillar of the upper coal seam is 90 m.

4.1. Stress Field Advance of the Working Face, Caused by Multi-Seam Mining

4.1.1. Deflection of the Principal Stress

Multi seam mining generally adopts a downward mining practice, so the relative position relationship between the underlying coal seam and the overlying coal seam mainly includes three types. Namely: external staggering (the end-mining line of the lower coal seam is under the gob of the upper coal seam), overlapping (the end-mining line of the upper and lower coal seams overlap), and internal staggering (the end-mining line of the lower coal seam is under the entity coal of the upper coal seam). Suppose the width of the final end-mining coal pillar of the lower coal seam is smaller than that of the upper coal seam. In that case, the working face of the lower coal seam will experience the whole process of the above three types of positional relationships.

The stress component of each point before each working face, is extracted through a numerical calculation. The maximum principal stress direction of the leading working face under three positional relations, is calculated using the stress component. It is specified that the angle of the maximum principal stress line rotating counterclockwise to the vertical direction line is "+" and vice versa is "−". The absolute value of the principal stress direction angle is less than 90°. When the upper and lower coal seams are at different off-set distances, the deflection characteristics of the principal stress of the element in the center of the lower coal seam with variable distances from the working face are shown in Figure 9.

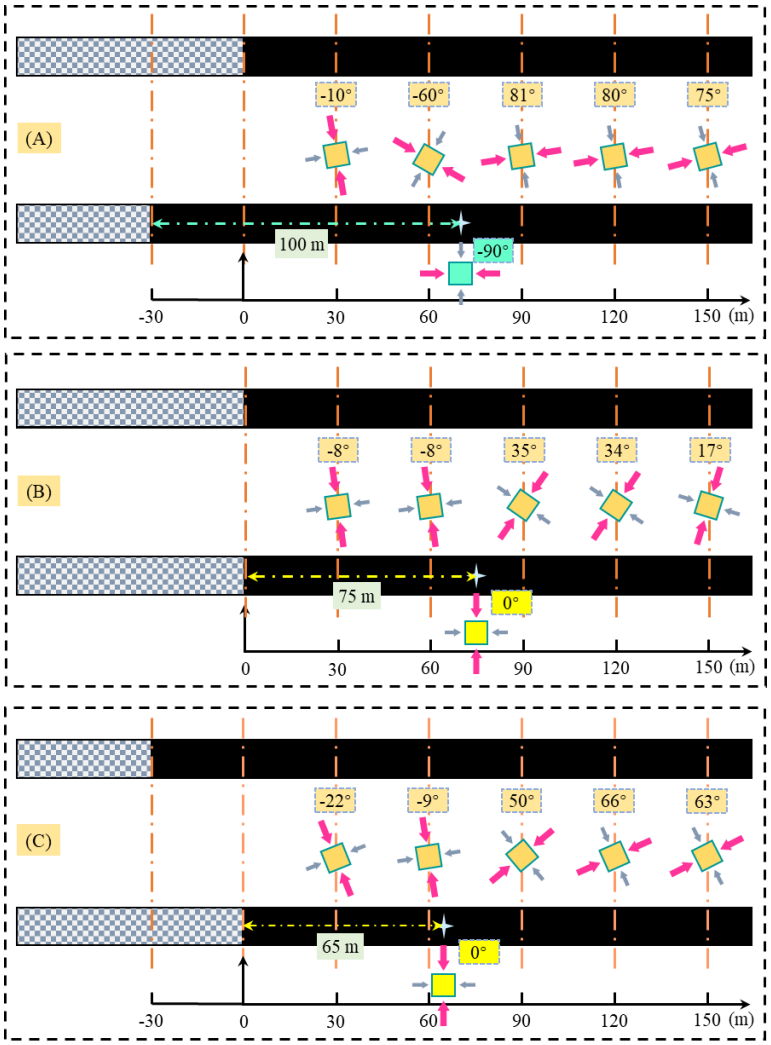

Figure 9. Deflection law of the principal stress in front of the different layout modes of the upper and lower coal seams. (**A**) External-offset of 30 m. (**B**) Overlapping arrangement. (**C**) Internal-offset of 30 m.

The primary conclusions are as follows.

(1) The external staggered arrangement differs from the overlapping and internal staggered arrangement. The evolution trajectory of the maximum principal stress direction is approximately vertical → horizontal → deflection to the vertical direction in the external staggered arrangement; while that in the overlapping and internal staggered arrangement is approximately vertical → vertical → inclined to the two ribs.

(2) The distance between the turning point of the maximum main stress direction (deflection angle of 0° or 90°) and the mining area, gradually decreases as the arrangement of the upper and lower coal seams changes from outer staggered type → overlap-

ping type → internal staggered type. It is reasonable to adopt symmetrical support measures for the roadway at the turning point of the principal stress.

(3) Under the condition of multi-seam mining, the maximum principal stress direction within 60 m in front of the lower coal seam is approximately vertical and deflected to the mining void. If the roadway is arranged here, the roadway surrounding rock will be damaged first along the direction of the minimum principal stress, namely the entity coal top angle of the roadway.

4.1.2. Direction Deflection of the Principal Stress

Under the influence of the repeated mining of multiple coal seams, the bearing stress in front of the workings will be subjected to the cyclic loading-unloading effect of mining stress. The geological rock body shows a typical non-homogeneity in the vertical stress direction, and the nature of the different rock seams varies. Therefore, the different relative positions of the upper and lower coal seams will significantly affect the peak and distribution characteristics of the stress field in front of the workings. The vertical stress of the model is selected as the index, and the distribution of the bearing stress field of the working face of the lower coal seam, when the upper and lower coal seams are at different staggered distances, is shown in Figure 10.

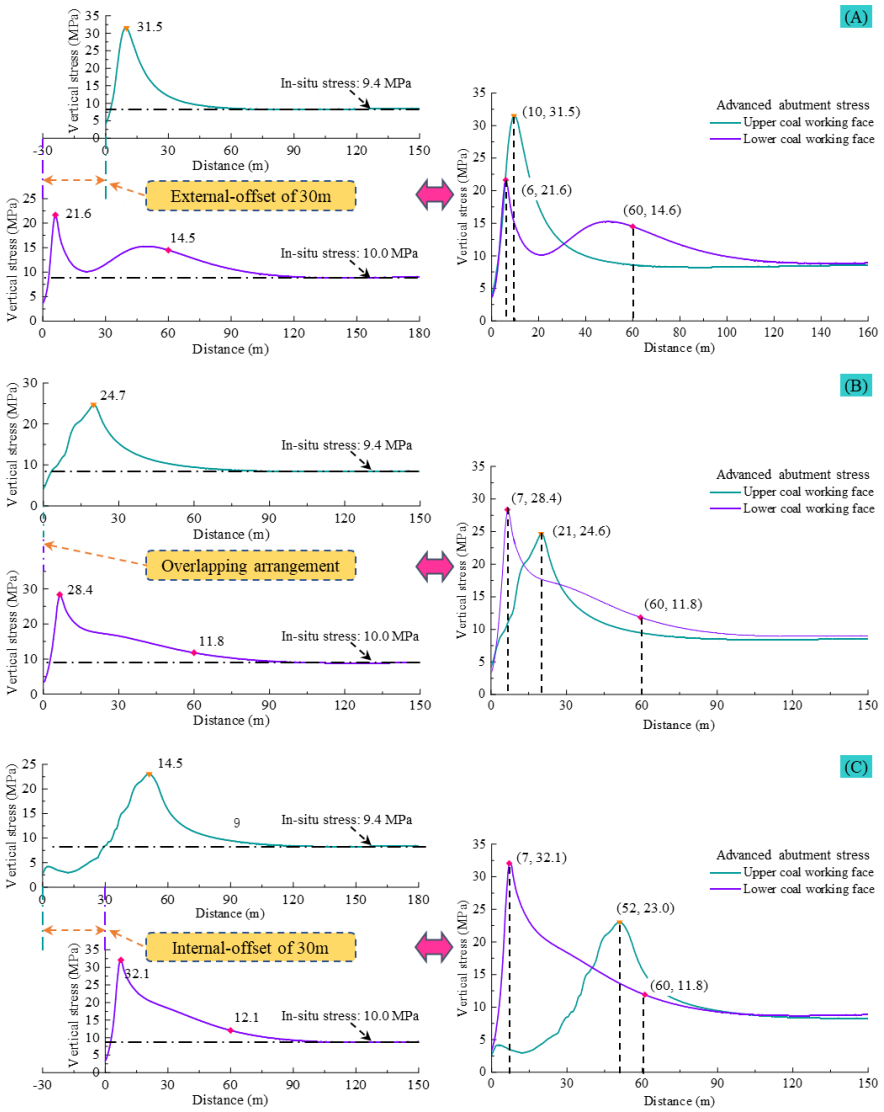

Figure 10. Abutment stress field distribution in the lower coal seam with different offset distances. (**A**) External-offset of 30 m. (**B**) Overlapping arrangement. (**C**) Internal-offset of 30 m.

As shown in Figure 10:

(1) When the working face is staggered outward, the upper and lower coal seam abutment stress shows a trend of increasing to the peak first, then gradually stabilizing. The peak stress ratio between the lower and upper coal seam is R_s = 0.69, and the depth ratio is R_d = 0.6. When the working face of the lower coal seam is ahead by 60 m, the loading factor of the peak stress, compared with the original rock stress is L = 1.46. Furthermore, the abutment stress curve of the working face of the lower coal seam shows double peak characteristics, due to the position of the working face of the upper coal seam.

(2) When the working face overlaps, the abutment stress trend in the upper and lower coal seams increases first and then decreases. The ratio of the peak stress between the lower coal seam and upper coal seam is R_s = 1.15, and the depth ratio is R_d = 0.33; when the working face of the lower coal seam is ahead by 60 m, the stress peak, compared to the original rock stress has a loading factor of L = 1.18.

(3) When the working face is staggered internally, the trend of the abutment stress in the upper and lower coal seams still increases first and then decreases. The ratio of the peak stress between the lower and upper coal seams is R_s = 1.40, and the depth ratio is R_d = 0.13; when the working face of the lower coal seam is ahead by 60 m, the loading factor of the peak stress, compared with the original rock stress is L = 1.18.

(4) In the process of the upper and lower working face from the outer fault → overlap → inner fault arrangement, the abutment stress peak of the lower coal seam working face increases continuously, and the value is gradually larger than that of the upper coal seam. The peak stress in the upper coal seam is the opposite of the peak stress in the upper coal seam. The peak stress depth of the lower coal seam does not change much and remains at a 6 to 7 m depth. In contrast, the peak stress depth in the upper coal seam is significantly affected by the working face layout, and the depth increases from 10 m to 52 m, an increase of 520%.

4.2. Roadway Group Stress Field Characteristics under Various Protective Coal Pillars

The relative positional relationship of the upper and lower coal seams working face significantly affects the abutment stress distribution condition in front of the working face. Due to the superimposed influence of the mining stress in multiple coal seams, the stress loading law of the main roadway group in the process of the upper and lower coal seams working face going from an outer staggered arrangement → overlapping arrangement → inner staggered arrangement, is significant for the selection of the width of the protection coal pillar. This section explores the stress evolution process of this seam's main roadway group affected by mining when the end-mining coal pillar of the upper coal seam is 90 m, with the gradual mining of the lower coal seam, as shown in Figure 11.

As shown in Figure 11:

(1) When the end-mining coal pillar of the upper coal seam is 90 m, the protective coal pillar's width of the lower coal seam main roadway reduces from ∞ m (which means that the lower coal seam is not mined) to 30 m, the abutment stress' peak of the lower coal seam main roadway group is gradually increasing. The maximum loading increase factor is L = 2.03. Furthermore, when the width of the coal pillar is less than 60 m (i.e., the overlapping arrangement of the upper and lower coal seams), the stress of the main roadway surrounding rock increases sharply.

(2) The surrounding rock of the main roadway group shows a typical asymmetric effect of the direction deflection of the stress and partial-stress boosting. The peak stress of the mining side is more extensive than its entity coal side of the main return-air roadway and main haulage roadway, and the degree of stress direction deflection and partial-stress boosting increases with the shortening of the end-mining coal pillar width. The direction deflection of stress and the partial-stress boosting phenomenon of the main roadway group surrounding rock shows that the stress distribution of the

surrounding rock is asymmetric, so it is necessary to use targeted support solutions in some places where the surrounding rock is weak.

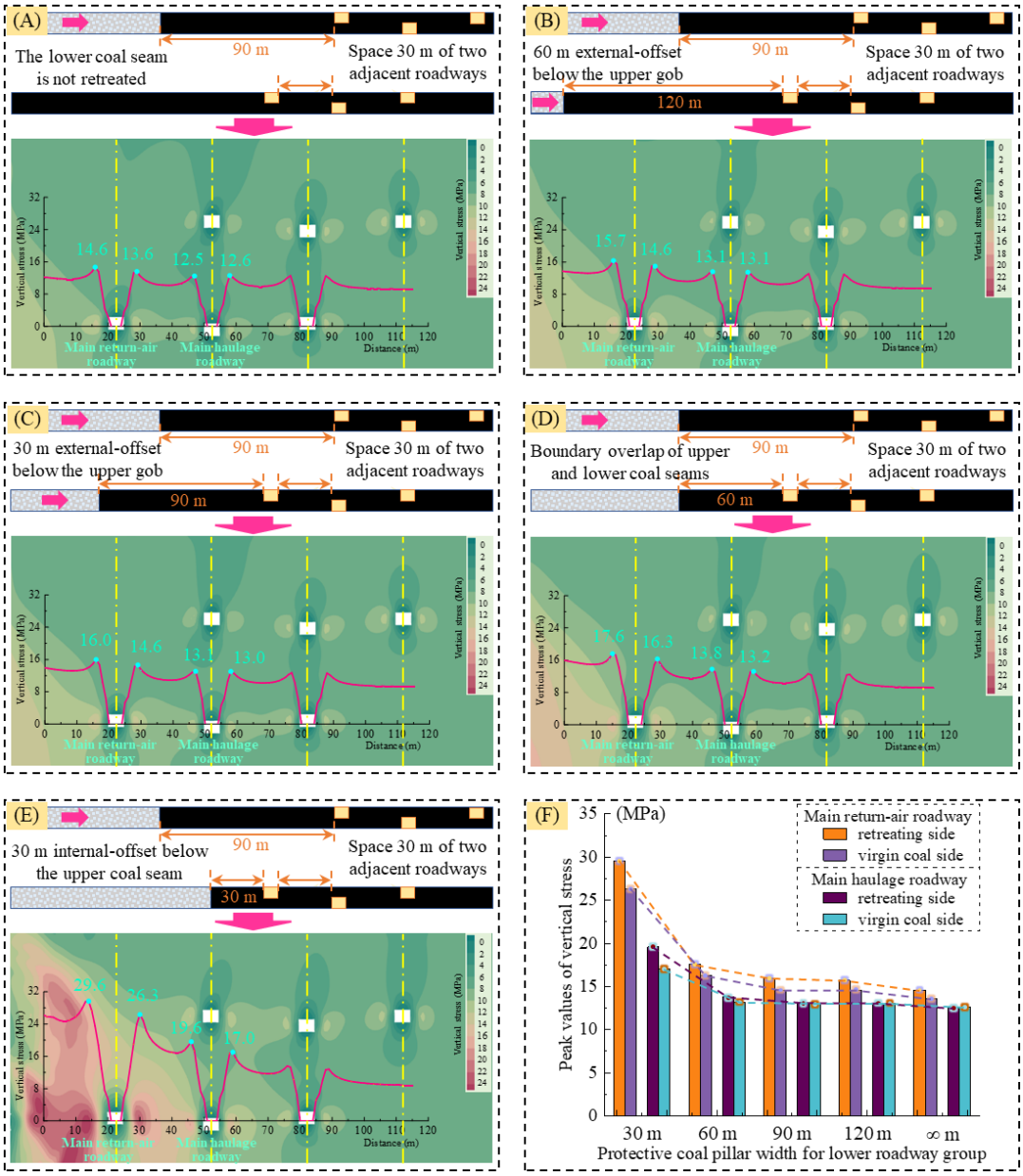

Figure 11. Stress evolution process of the main roadway group during the lower coal seam recovery. (**A**–**E**) with the protective coal pillar widths of ∞ m, 120 m, 90 m, 60 m, and 30 m, respectively, and (**F**) distribution of peak stress value in both ribs.

4.3. Law of Stress Direction Deflection and Partial-Stress Boosting of the Deviatoric Stress Field of the Surrounding Rock with Different End-Mining Coal Pillar Widths

Deviatoric stress is the stress that deviates from hydrostatic stress and causes deformation, reflecting the essence of plastic deformation at a point in the surrounding rock. The high deviatoric stress area in the surrounding rock indicates that the area is in a state of damage development. Mining activities, especially the disturbance of multi-seam mining, will promote the direction deflection of stress and partial-stress boosting effect of the main roadway surrounding rock, further leading to the formation and transfer of the high deviatoric stress zone in the surrounding rock. It is of great significance to investigate the development and evolution of the high deviatoric stress zone in the surrounding rock

to develop the damage mechanism and key reinforcement technology of the roadway surrounding rock. This section explores the evolution of the peak deviatoric stress zone and plastic zone of this seam's main roadway group affected by mining when the end-mining coal pillar width of the upper coal seam is 90 m, with the gradual mining of the lower coal seam, as shown in Figure 12.

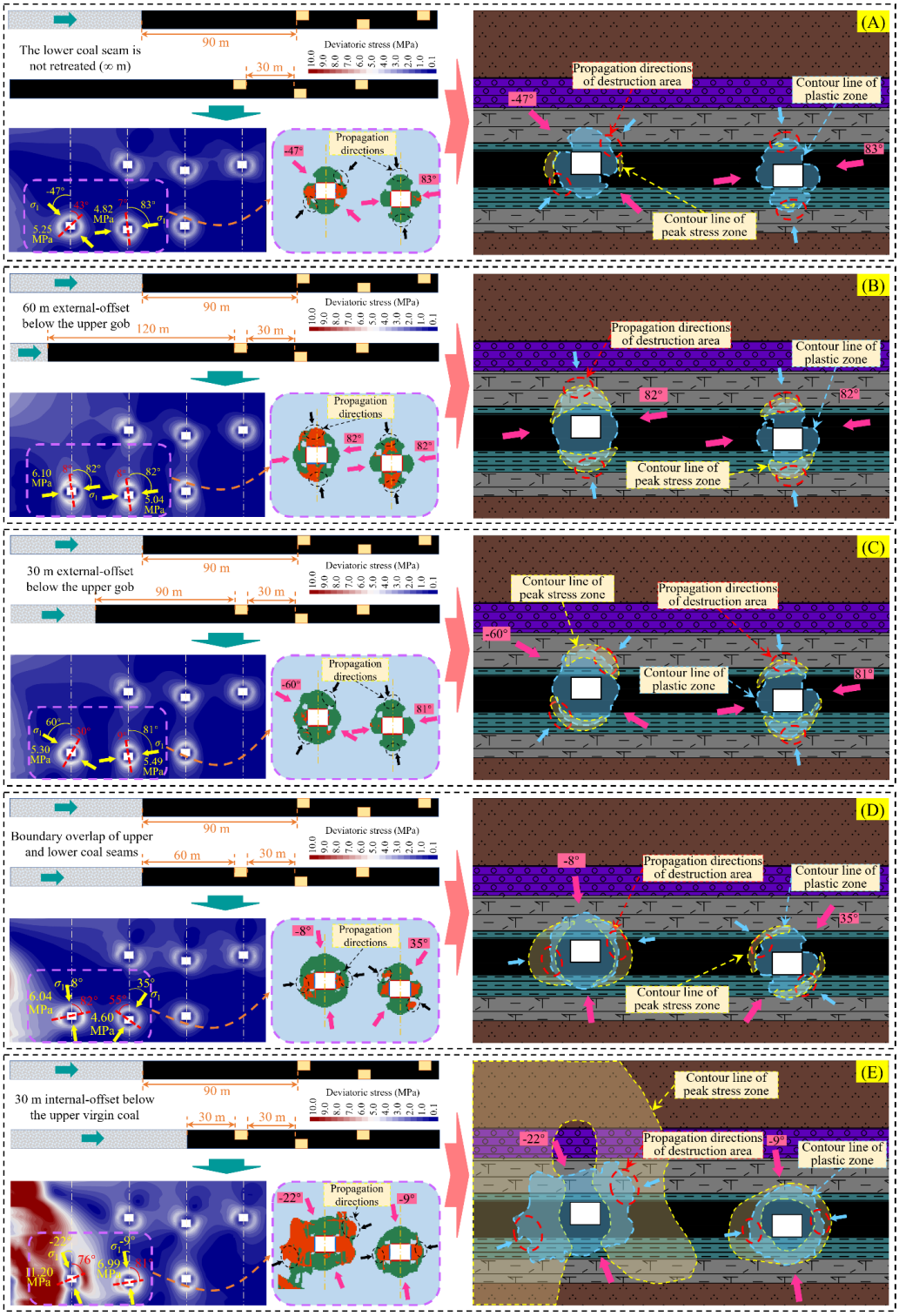

Figure 12. Development characteristics of the deviatoric stress peak zone and plastic zone. (**A**–**E**) with the protective coal pillar widths of ∞ m, 120 m, 90 m, 60 m, and 30 m, respectively.

As shown in Figures 12 and 13:

(1) The peak value of deviatoric stress shows an overall increasing trend with advancing the lower coal seam workings. When the width of the end-mining coal pillar is from ∞ m → 60 m → 30 m, the peak value of deviatoric stress in the main return-air roadway is from 5.25 MPa → 6.04 MPa → 11.20 MPa. The maximum stress loading factor is L = 2.1, and the peak value of the deviatoric stress in the main haulage roadway is from 4.82 MPa → 4.60 MPa → 6.99 MPa, and the maximum stress loading factor is L = 1.45. When the width of the lower end-mining coal pillar is more than 60 m, the peak value of the deviatoric stress in the main roadway group is more fluctuating. When the width of the lower end-mining coal pillar is bigger than 60 m, the peak value of the deviatoric stress in the main roadway group is more fluctuating, indicating that the peak distribution is not significantly affected by the larger width of the end-mining coal pillar.

(2) The peak deviatoric stress area gradually expands during the gradual decrease of the lower coal seam end-mining coal pillar width. As the influence of mining intensifies, the peak deviatoric stress area gradually surrounds the roadway surrounding rock and shows an apparent directional deflection. The location of the peak zone gradually transitions from the roof and floor to both ribs of the roadway. The plastic zone's contour line of the roadway passes through the core area of the peak of the deviatoric stress. Furthermore, the plastic zone evolution direction also has obvious directionality; with the minimum principal stress direction deflection, the plastic zone development position occurs with a corresponding shift.

(3) The maximum principal stress direction shows a significant deflection with the advancing lower coal seam workings (main return-air roadway). With the increase of the distance of the main roadway from the gob area, the direction of the maximum principal stress gradually transitions from the direction of the deflected gob area to the direction of the deflected entity coal. The direction of the minimum principal stress passes through the center of the peak deviatoric stress area of the two ribs of the roadway. The location of the peak of the deviatoric stress shows a significant asymmetry, and this type is to be avoided in the actual project.

(4) When the width of the end-mining coal pillar in the lower seam is 60 m, the direction of the maximum principal stress of the main return-air roadway is approximately perpendicular to the roof and floor of the roadway (deflected 8° toward the side of the gob area). That means the direction of the minimum principal stress in the roadway points to the entity coal top angle of the roadway, which also corresponds to the direction of the development of the plastic zone in the roadway. The failure results of the main roadway by a numerical simulation are consistent with the failure position of the main roadway under field working conditions, and the failure mechanism of the surrounding rock of the roadway is well revealed. This is conducive to applying an early warning and asymmetric control technology for the deformation orientation of the main roadway surrounding rock.

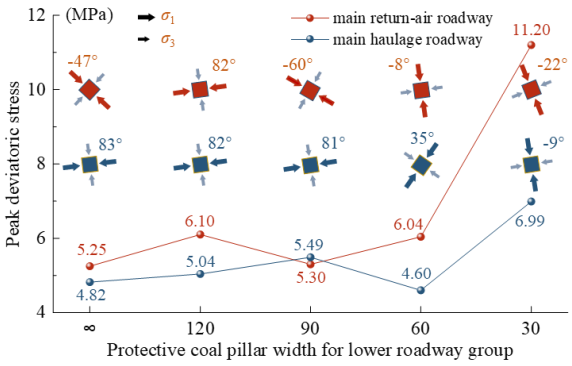

Figure 13. Stress distribution of the main roadway group in the lower coal seam.

5. Surrounding Rock Control Techniques

5.1. Principle of the Asymmetric Reinforcement Support Cooperation

In the process of the lower coal seam mining, with the reduction of the width of the protective coal pillar of the main roadway group, the principal stress magnitude and direction will change in the main roadway surrounding rock. In the process of the mining influence, there is critical area of the direction deflection of stress and partial-stress boosting in the main roadway surrounding rock, and the area of the direction deflection of the stress and partial-stress boosting is the peak area of the deviatoric stress in the main roadway surrounding rock, which is also the precursor and leading area for the development of damage or continuous damage in the surrounding rock. Thus, the principle of the asymmetric directional cooperative anchorage in the critical area of the stress direction deflection and the partial-stress boosting, is proposed in the roadway surrounding rock. Based on the evolution process of the stress direction deflection and the partial-stress boosting area of the roadway surrounding rock, a directional high prestressing anchorage reinforcement technology is adopted to realize the synergistic anchorage with the original support scheme and guarantee the stability of the main roadway group.

Based on the study mentioned above, the multi-coal seam mining disturbance leads to a significant change in the magnitude and directional deflection of the principal stress. In a comprehensive view, there are three main categories of the deflected load critical areas in the upper and lower coal seam main roadway: two ribs area, roof area, floor area, and rib angle area (two types). The critical area of the directional cooperative anchorage is the peak area of the deviatoric stress, the key area of the stress direction deflection and the partial-stress boosting of the main roadway surrounding rock. For this reason, four types of essential roadway surrounding rock reinforcement anchorage schemes are proposed for the different degrees of the direction deflection of the stress and partial-stress boosting, as shown in Figure 14.

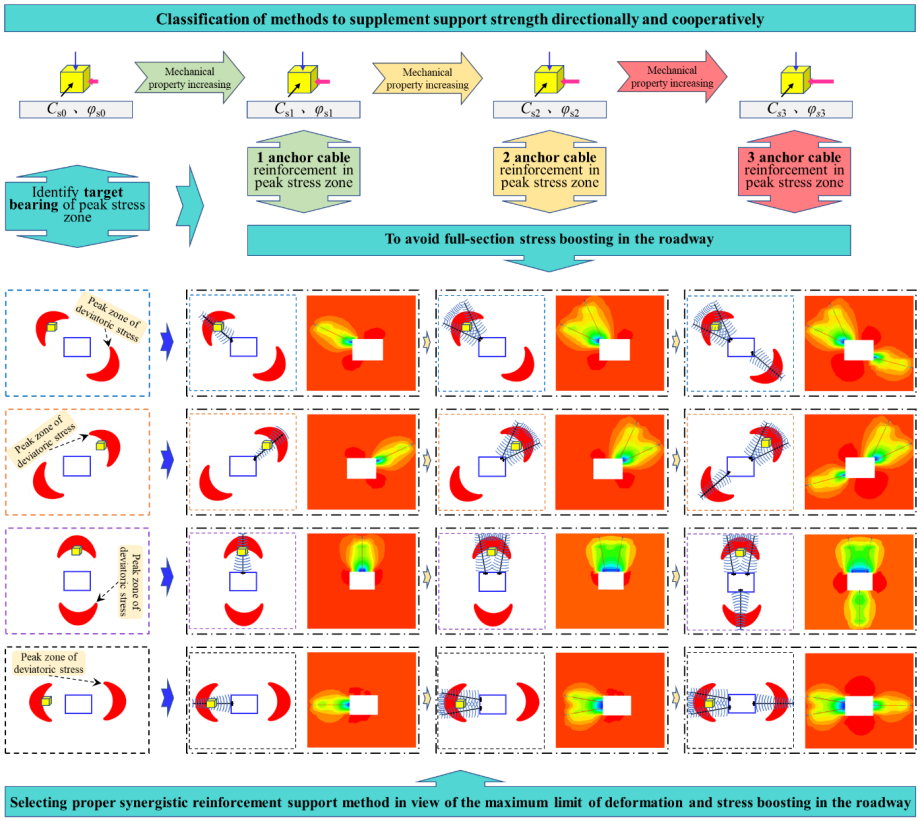

Figure 14. Principle of the directional cooperative anchoring in the roadway.

In the principle of the high pre-stressed anchor cable reinforcement anchoring effect, the average equivalent mechanical parameters of the surrounding rock in the critical area of the stress direction deflection and the partial-stress boosting can be increased from C_{s0} and φ_{s0} to the equivalent C_{s1} and φ_{s1}, C_{s2} and φ_{s2}, or C_{s3} and φ_{s3}, by the high prestress and high shear failure resistance provided by the anchor cable, where $C_{s3} > C_{s2} > C_{s01} > C_{s0}$ and $\varphi_{s3} > \varphi_{s02} > \varphi_{s01} > \varphi_{s0}$. This means that the mechanical properties of the surrounding rocks in the key zone of the direction deflection of the stress and partial-stress boosting are strengthened to improve the overall bearing capacity of the surrounding rocks of the main roadway.

5.2. Support Parameters

Based on the principle mentioned above of the directional cooperative anchoring of the roadway, a targeted support scheme is put forward for the main return-air roadway of the No.3 coal seam. Based on the original support scheme, two anchor cables are additionally supported on the mining side of the roadway, with an angle of 15° with the horizontal, the anchor cable specification of Φ17.8 × 7000 mm, and the row spacing of 1500 mm × 2000 mm. The same row of anchor cables and each row of anchor cables are connected with the W steel strip, respectively, forming a crisscross net-like combined support structure, increasing the surface stress range of the roadway surrounding rock. Add one anchor cable of Φ17.8 × 7000 mm with 2000 mm row spacing on the entity coal side and the W steel strip connects each row of the anchor cables. Detailed support parameters are shown in Figure 15.

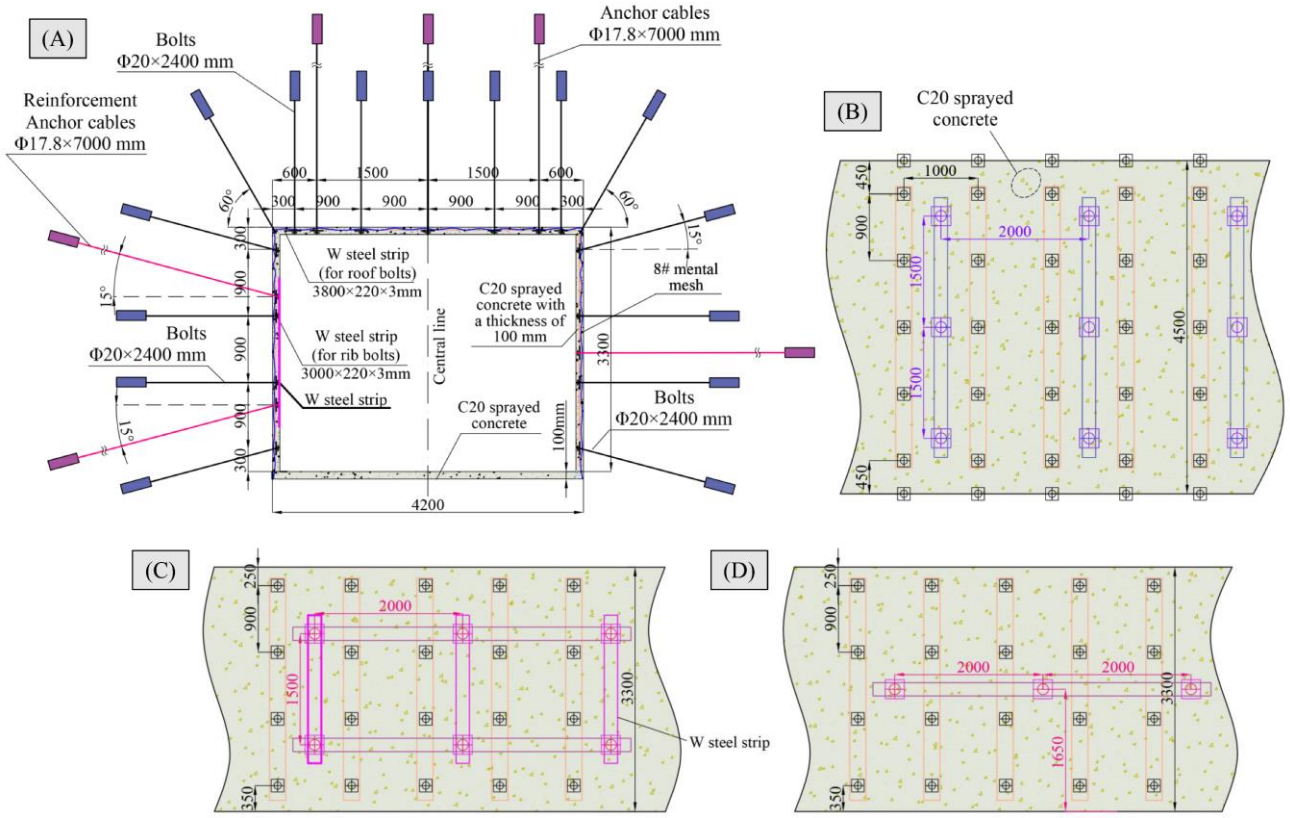

Figure 15. No. 3 coal seam main return-air roadway reinforcement support program. (**A**) Entry section. (**B**) Support pattern in roof. (**C**) Support patter in coal pillar rib. (**D**) Support pattern in virgin coal rib.

In order to further analyze the rationality of the directional cooperative anchoring support scheme, the support stress field of the No. 3 coal seam main return-air roadway is shown in Figure 16. A deep compressive stress zone and a shallow core compressive stress

zone are formed in the surrounding rock after adopting the bolt-cable combined support. The stress field of the anchor rods of the two ribs avoided the fall of the broken surrounding rock of the roadway surface but did not form a practical strengthening effect on the peak area of the deviatoric stress. The principle of support reinforcement is shown in Figure 17. Following the use of the asymmetric reinforcement support with anchor cables, the channel steel anchor cable reinforced mining rib formed two functional compressive stress areas in the center of the deviated stress core area. This can effectively deliver the external mining stress of the surrounding rock to the deep elastic rock, thus inhibiting the damage to the roadway surrounding rock in this area.

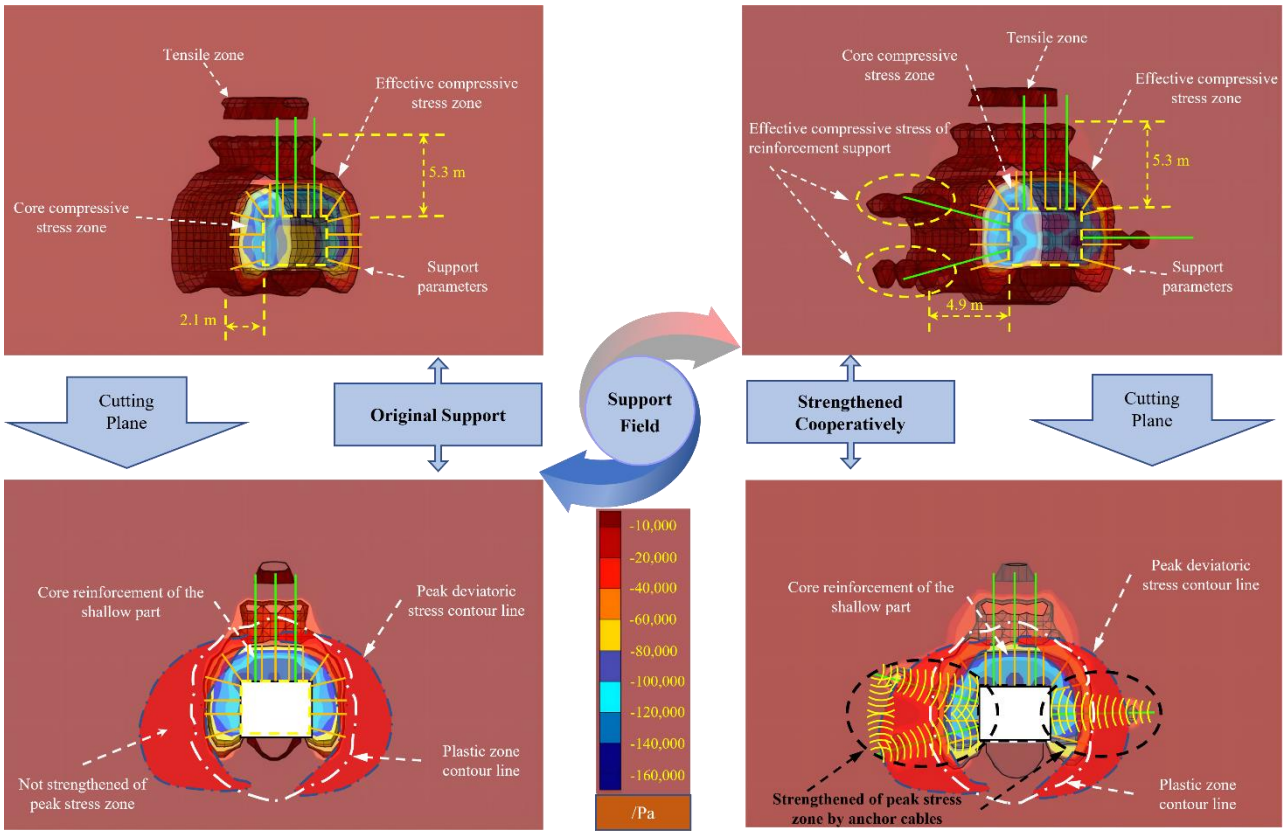

Figure 16. No.3 coal seam main return-air roadway support stress field.

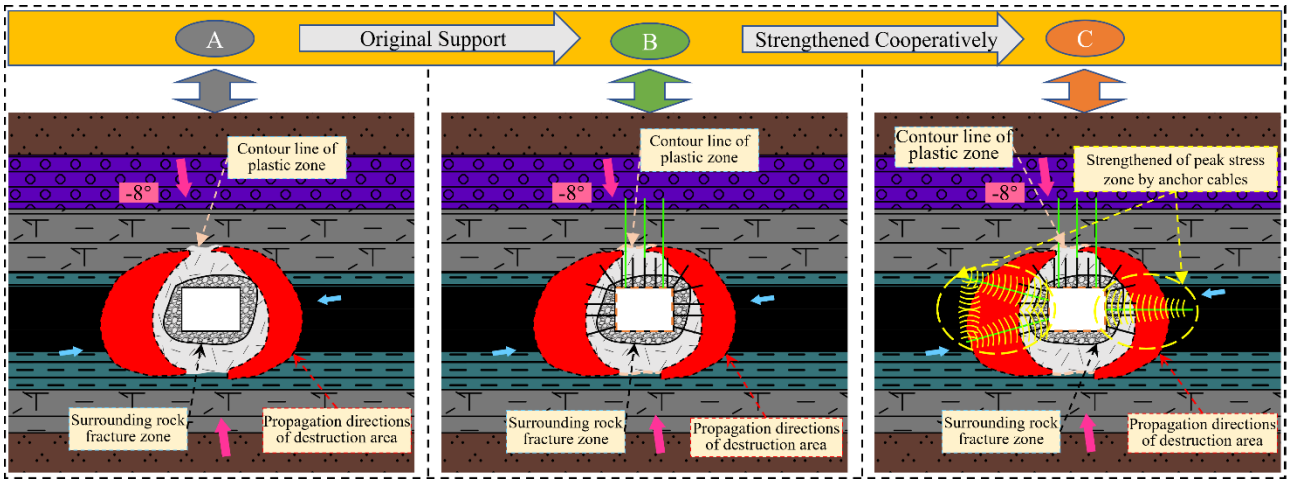

Figure 17. The support reinforcement principle of the No.3 coal seam main return-air roadway. (**A**) No support. (**B**) Original support. (**C**) Strengthen support.

5.3. Ground Pressure Monitoring

To analyze the mining pressure response of the working face and the return-air roadway of this coal seam during the pushing process of the C3# coal seam, we arranged three measurement stations (each with an interval of 15 m) along the axis of the working face return-air road and the C3# coal seam return-air roadway, respectively. The observation indexes of the stations are mainly: (1) the abutment stress of the mining roadway; (2) the stress of the bolts in the mining roadway and main roadway; (3) the amount of surrounding rock displacement. The changing trend of these indicators is analyzed to reveal further the law of change of the stress field in the surrounding rock of the main roadway when the width of the protective coal pillar is different, to determine the width of the protective coal pillar in the main roadway of LWF 8216. The monitoring principle is as Figure 18.

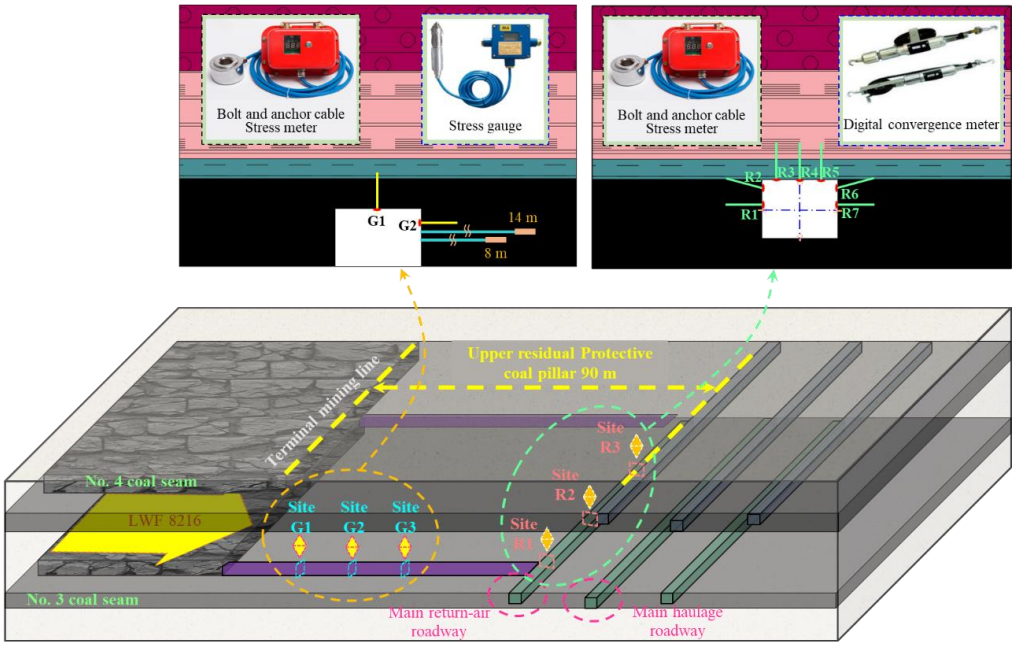

Figure 18. Ground pressure monitoring arrangement.

The location of the drilling stress monitoring is the C3# coal seam working face mining roadway. Each measurement point has two stress gauges, A and B, where A is 14 m deep into the coal body, and B drill holes are 8 m deep into the coal body. The results of the LWF 8216 track roadway's abutment stress monitoring are shown in Figure 19.

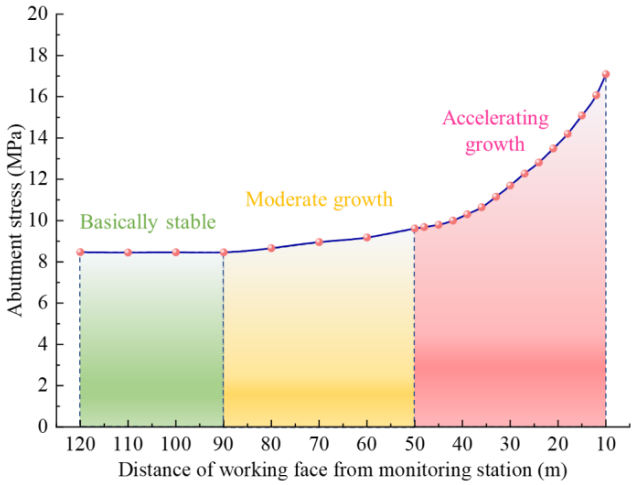

Figure 19. Monitoring results of the deep hole stress meters.

When the distance between the working face and the stress meter is more than 90 m, the reading of the stress meter is stable, and there is no apparent stress-increasing trend. However, the reading shows a slow and slightly increasing trend when the working face is 90~50 m from the stress meter. When the distance between the working face and the stress meter is less than 50 m, and the face is closer to the monitoring section of the high-sensitivity borehole stress station, the abutment stress value begins to show an apparent acceleration trend in front of the working face.

The anchor cable support resistance can reflect the deformation state of the roadway surrounding rock and the influence of the working face in real time. It can effectively determine the reasonable width of the end-mining coal pillar of the main roadway group. Monitoring stations were set up in the LWF 8216 track roadway, and the C3# coal seam main return-air roadway, respectively, and the stress meters were arranged, as in Figure 18; the monitoring results are shown in Figure 20.

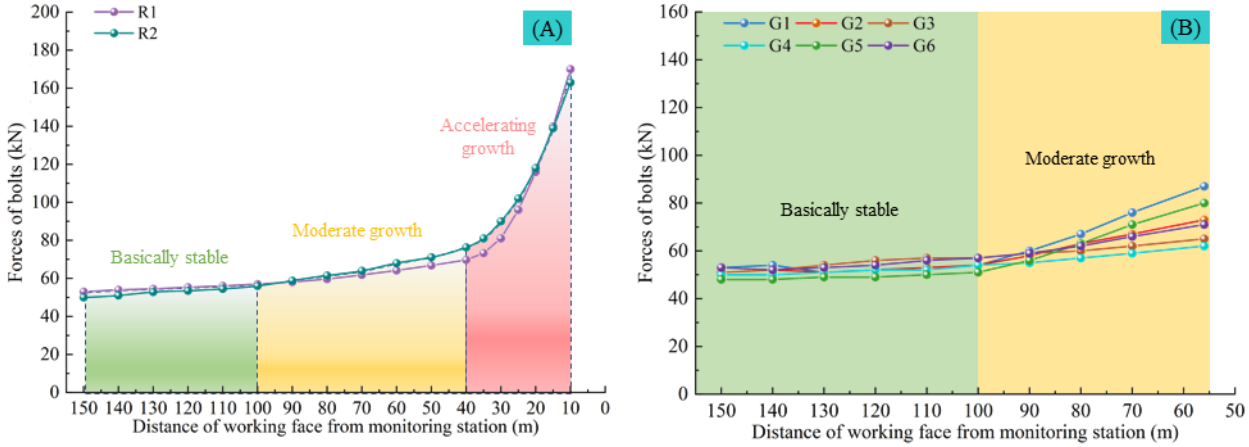

Figure 20. Anchor bolts stress meter monitoring results. (**A**) The main haulage roadway. (**B**) The main return-air roadway.

The pre-stress range of the anchor bolts in the LWF 8216 track roadway is 50~53 KN. The values of the stress meters are 163~170 KN after the working face is stopped mining and is stabilized, which is about 90.6~94.4% of its breaking load, and still in a safe working condition; with the decrease of the distance between the working face and the anchor meter, the values of stress meters goes through the process of basic stability (more than 100 m) $\rightarrow$ slow increase (100~40 m) $\rightarrow$ accelerated increase (less than 40 m). This indicates that the stress of the advanced mining will be significantly enhanced within 40 m in front of the working face.

In the C3# coal seam main return-air roadway, the anchor pre-stress values range from 49 to 53 KN. Once the working face has stopped mining 56 m from the main roadway, the anchor stress meter of the main roadway showed an apparent asymmetry, and the values of the two ribs were significantly larger than the roof. With the decrease of the distance between the working face and the anchor bolts stress meter, the values of stress meters went through the process of a primary stability (greater than 100 m) $\rightarrow$ slow rise (100~56 m), and the final value of the stress meters was about 34.4.0~48.3% of its breaking load. The comparison and analysis of the values of the stress meters (G1~G6), G1 > G2 > G5, G6 > G3 > G4, show that the surrounding rock of the two sides of the main roadway, especially the mining side, is more sensitive to the mining effect of the working face. The field monitoring results are consistent with the numerical simulation results of the critical control area of the surrounding rock, indicating that the theory of the stress direction deflection and the partial-stress boosting of the surrounding rock is suitable for early warning and strengthening the support of the surrounding rock deformation.

6. Conclusions

In this paper, the theoretical analysis, numerical simulation, and on-site ground pressure monitoring are used to study the effects of the partial-stress boosting and the direction deflection of the stress field on the failure evolution of the surrounding rock. The conclusions are as follows:

(1) Mining-induced stress prompted two modes of critical zones of the deviatoric stress in the roadway. When the extent of the partial-stress boosting is weak, the critical zones of the deviatoric stress in the roadway mainly developed symmetrically in two directions of the roadway. While the extent of the partial-stress boosting was strong, the critical zones of the deviatoric stress were symmetrically distributed on both sides of the roadway, and the damaged area tended to develop from four directions to the deep part of the surrounding rock.

(2) With the influence of the multi-seam mining activities, the stress fields in the main roadway showed an asymmetric effect of the partial-stress boosting, and as the end-mining coal pillar width in the lower coal seam was shortened, the extent of partial-stress boosting increased. The direction of the maximum principal stress in the roadway showed a significant characteristic of deflection, and the peak points of the stress field were asymmetrically distributed.

(3) On-site mine pressure monitoring showed that when the upper and lower working faces overlapped, the mining stress tended to be significantly enhanced in the range of 40~50 m in front of the lower coal seam working face. Once the lower working face was stopped at 56 m from the main roadway, the surrounding rock of both ribs, especially the mining side, was more sensitive to the impact of mining.

Author Contributions: Conceptualization, D.C.; Data curation, Z.L.; Formal analysis, Z.L. and X.M.; Funding acquisition, D.C.; Investigation, X.M., Y.W. and Z.W.; Methodology, D.C., F.G. and S.X.; Project administration, D.C. and S.X.; Software, D.C., F.G., Z.L., X.M. and Y.W.; Supervision, S.X.; Validation, Y.W. and Z.W.; Writing–original draft, D.C., F.G. and Z.L. Writing–Review and Editing, D.C., F.G. and Z.L. All authors have read and agreed to the published version of the manuscript.

Funding: This work was financially supported by the National Natural Science Foundation of China (Grant No. 52004286), the Fundamental Research Funds for the Central Universities (Grant No. 2022XJNY02), the China Postdoctoral Science Foundation (Grant No. 2020T130701, 2019M650895), all of which were gratefully acknowledged.

Conflicts of Interest: The authors declare no conflict of interest.

References

1. Jia, H.; Li, T.; Wang, A.; Liu, G.; Guo, X. Decoupling analysis of economic growth and mineral resources consumption in China from 1992 to 2017: A comparison between tonnage and exergy perspective. *Resour. Policy* **2021**, *74*, 102448. [CrossRef]
2. Zou, C.; Xiong, B.; Xue, H.; Zheng, D.; Ge, Z.; Wang, Y.; Jiang, L.; Pan, S.; Wu, S. The role of new energy in carbon neutral. *Pet. Explor. Dev.* **2021**, *48*, 480–491. [CrossRef]
3. Cao, J.W.; Zhang, W.; Li, Y.; Zhao, C.; Zheng, Y.; Yu, B. Current Status of Hydrogen Production in China. *Prog. Chem.* **2021**, *33*, 2215–2244. [CrossRef]
4. Jiachen, W.; Peng, S.; Yang, L. State of the art in underground coal mining and automation technology in the United States. *J. China Coal Soc.* **2021**, *46*, 36–45. [CrossRef]
5. Peng, S.S.; Du, F.; Cheng, J.Y.; Li, Y. Automation in U.S. longwall coal mining: A state-of-the-art review. *Int. J. Min. Sci. Technol.* **2019**, *29*, 151–159. [CrossRef]
6. Ghosh, N.; Agrawal, H.; Singh, S.K.; Banerjee, G. Optimum Chain Pillar Design at the Deepest Multi-Seam Longwall Workings in India. *Min. Metall. Explor* **2020**, *37*, 651–664. [CrossRef]
7. Bruce, H.; Jim, G. A review of the geomechanics aspects of a double fatality coal burst at Austar Colliery in NSW, Australia in April 2014. *Int. J. Min. Sci. Technol.* **2017**, *27*, 3–7. [CrossRef]
8. Pariseau, W.G.; Larson, M.K.; Lawson, H.E.; Tesarik, D.R. User-friendly finite element design of main entries, barrier pillars, and bleeder entries. *Int. J. Min. Sci. Technol.* **2018**, *28*, 3–10. [CrossRef]
9. Gao, F.Q.; Stead, D.; Kang, H.P.; Wu, Y.Z. Discrete element modelling of deformation and damage of a roadway driven along an unstable goaf-A case study. *Int. J. Coal Geol.* **2014**, *127*, 100–110. [CrossRef]

10. Gao, F.; Stead, D.; Kang, H. Simulation of roof shear failure in coal mine roadways using an innovative UDEC Trigon approach. *Comput. Geotech.* **2014**, *61*, 33–41. [CrossRef]
11. Gao, F.Q.; Stead, D.; Kang, H.P. Numerical Simulation of Squeezing Failure in a Coal Mine Roadway due to Mining-Induced Stresses. *Rock Mech. Rock Eng.* **2015**, *48*, 1635–1645. [CrossRef]
12. Wang, X.F.; Wang, J.Y.; Chen, X.Y.; Chen, Z.C. A Roadway In Close Distance to coal seam in deep mine: Location selection and supporting practice based on creep characteristics of surrounding rocks. *Arch. Min. Sci.* **2021**, *66*, 407–419. [CrossRef]
13. Pan, S.Q.; Liu, S.T.; Cao, L.M.; Guo, J.Q.; Yuan, C. Deformation Failure and Support Test of Surrounding Rock in Deep Arched Roadway with Straight Wall. *Adv. Civ. Eng.* **2021**, *2021*, 11. [CrossRef]
14. Mohammadi, H.; Ebrahimi Farsangi, M.A.; Jalalifar, H.; Ahmadi, A.R. A geometric computational model for calculation of longwall face effect on gate roadways. *Rock Mech. Rock Eng.* **2016**, *49*, 303–314. [CrossRef]
15. Huang, B.; Zhang, N.; Jing, H.; Kan, J.; Meng, B.; Li, N.; Xie, W.; Jiao, J. Large deformation theory of rheology and structural instability of the surrounding rock in deep mining roadway. *J. China Coal Soc.* **2020**, *45*, 911–926.
16. Xiong, Y.; Kong, D.; Cheng, Z.; Wen, Z.; Ma, Z.; Wu, G.; Liu, Y. Instability Control of Roadway Surrounding Rock in Close-Distance Coal Seam Groups under Repeated Mining. *Energies* **2021**, *14*, 5193. [CrossRef]
17. Shan, R.; Peng, Y.; Kong, X.; Li, H. Research progress of coal roadway support technology at home and abroad. *Chin. J. Rock Mech. Eng.* **2019**, *38*, 2377–2403.
18. Chen, D.; Xie, S.; Wu, Y.; Guo, F.; He, F.; Liu, R. Reasonable location of stopping line in close-distance underlying coal seam and partition support of large cross-section roadway. *Int. J. Coal. Sci. Technol. 9*. [CrossRef]
19. Yuan, W.; Hong, K.; Liu, R.; Ji, L.; Meng, L. Numerical Simulation of Coupling Support for High-Stress Fractured Soft Rock Roadway in Deep Mine. *Adv. Civ. Eng.* **2022**, *16*, 1–10.
20. Yuan, Y.; Wang, W.J.; Yuan, C.; Yu, W.J.; Peng, W.Q. Large deformation failure mechanism of surrounding rock for gateroad under dynamic pressure in deep coal mine. *J. China Coal Soc.* **2016**, *41*, 2940–2950.
21. Xie, S.; Wang, E.; Chen, D.; Jiang, Z.; Li, H.; Liu, R. Collaborative control technology of external anchor-internal unloading of surrounding rock in deep large-section coal roadway under strong mining influence. *J. China Coal Soc.* **2022**, *47*, 1946–1957.
22. Liu, S.; Yang, K.; Tang, C. Asymmetric failure mechanism and control of downhill roadway group of soft rock in deep mine. *J. Min. Saf. Eng.* **2019**. [CrossRef]
23. Li, G.; Sun, Y.; Zhang, J.; Zhang, Q.; Sun, C.; Zhang, S.; Bi, R. Experiment and application of coalcrete on roadway stability: A comparative analysis. *Adv. Mater. Sci. Eng.* **2020**, *2020*, 1–14. [CrossRef]
24. Sun, Y.; Bi, R.; Sun, J.; Zhang, J.; Taherdangkoo, R.; Huang, J.; Li, G. Stability of roadway along hard roof goaf by stress relief technique in deep mines: A theoretical, numerical and field study. *Geomech. Geophys. Geo-Energy Geo-Resour.* **2022**, *8*, 1–16. [CrossRef]
25. Xie, S.; Guo, F.; Wu, Y. Control Techniques for Gob-Side Entry Driving in an Extra-Thick Coal Seam with the Influence of Upper Residual Coal Pillar: A Case Study. *Energies* **2022**, *15*, 3620. [CrossRef]
26. Wang, E.; Xie, S. Determination of coal pillar width for gob-side entry driving in isolated coal face and its control in deep soft-broken coal seam: A case study. *Energy Sci. Eng.* **2022**, *10*, 2305–2316. [CrossRef]
27. Zhang, Z.; Bai, J.; Chen, Y.; Yan, S. An innovative approach for gob-side entry retaining in highly gassy fully-mechanized longwall top-coal caving. *Int. J. Rock Mech. Min. Sci.* **2015**, *80*, 1–11. [CrossRef]
28. Chen, D.; Guo, F.; Xie, S.; Wang, E.; Wu, Y.; Jiang, Z.; Wang, L.; Cui, J.; Zhang, X.; Liu, R. Mining-induced failure characteristics and surrounding rock control of gob-side entry driving adjacent to filling working face in the deep coal mine. *Energy Sci. Eng.* **2022**, *10*, 2593–2611. [CrossRef]
29. Wu, R.; Zhang, P.; Kulatilake, P.H.S.W.; Luo, H.; He, Q. Stress and deformation analysis of gob-side pre-backfill driving procedure of longwall mining: A case study. *Int. J. Coal. Sci. Technol.* **2021**, *8*, 1351–1370.
30. He, F.L.; Lv, K.; Li, X.B.; Qin, B.B.; Li, L. Failure Mechanism and Control of Lower Retracement Channel in Close-Distance Double-Thick Coal Seams. *Shock Vib.* **2021**, *2021*, 1–19. [CrossRef]
31. Wu, W.-D.; Bai, J.-B.; Wang, X.-Y.; Yan, S.; Wu, S.-X. Numerical Study of Failure Mechanisms and Control Techniques for a Gob-Side Yield Pillar in the Sijiazhuang Coal Mine, China. *Rock Mech. Rock Eng.* **2018**, *52*, 1231–1245. [CrossRef]
32. Sun, Y.; Bi, R.; Chang, Q.; Taherdangkoo, R.; Zhang, J.; Sun, J.; Huang, J.; Li, G. Stability Analysis of Roadway Groups under Multi-Mining Disturbances. *Appl. Sci.* **2021**, *11*, 7953. [CrossRef]
33. Yang, S.; Li, G.; Bi, R.; Yao, B.; Feng, R.; Sun, Y. The Stability of Roadway Groups under Rheology Coupling Mining Disturbance. *Sustainability* **2021**, *13*, 12300. [CrossRef]
34. Wang, W.; Yuan, C.; Yu, W.; Wu, H.; Peng, W.; Peng, G.; Liu, X.; Dong, E. Stability control method of surrounding rock in deep roadway with large deformation. *J. China Coal Soc.* **2016**, *41*, 2921–2931.
35. Barber, J.R. *Elasticity*; Springer: Berlin/Heidelberg, Germany, 2002.
36. Zhilun, X. *Elasticity*; Beijing Higher Education Publishing House: Beijing, China, 2006.
37. Qian, M.; Xu, J.; Wang, J. *Ground Pressure and Strata Control*; China University of Mining and Technology Press: Beijing, China, 2021.
38. Xiong, L.-X.; YU, L.-J. Comparative study of three Mohr strength criteria. *J. Yangtze River Sci. Res. Inst.* **2016**, *33*, 81.
39. Cai, M.F.; He, M.C.; Liu, D. *Rock Mechanics and Engineering*; Science Press: Beijing, China, 2013.
40. Mohammad, N.; Reddish, D.; Stace, L. The relation between in-situ, and laboratory rock properties used in numerical modelling. *Int. J. Rock Mech. Min. Sci.* **1997**, *34*, 289–297. [CrossRef]

41. Medhurst, T.; Brown, E. A study of the mechanical behaviour of coal for pillar design. *Int. J. Rock Mech. Min. Sci.* **1998**, *35*, 1087–1105. [CrossRef]
42. Hoek, E.; Brown, E. The Hoek–Brown failure criterion and GSI–2018 edition. *J. Rock Mech. Geotech. Eng.* **2019**, *11*, 445–463. [CrossRef]
43. Hoek, E.; Brown, E.T. Empirical strength criterion for rock masses. *J. Geotech. Eng. Div.* **1980**, *106*, 1013–1035. [CrossRef]